Supporting Information

Twin Boundary $Cd_xZn_{1-x}S$: A New Anode for High Reversibility and Stability Lithium/Sodium-Ion Batteries

Zhen Kong[a,b†], Meiling Huang[a,b†], Kang Zhang[b], Zhenyan Liang[b], Huayao Tu[b], Yongliang Shao[a,b], Yongzhong Wu[a,b,*], Xiaopeng Hao[a,b,*]

a. School of Materials Science and Engineering, Qilu University of Technology (Shandong Academy of Science), Jinan, 250353, P. R. China;

b. State Key Lab of Crystal Materials, Shandong University, Jinan 250100, P. R. China.

† These authors contributed equally to this work.

*Corresponding author: E-mail: wuyz@sdu.edu.cn; xphao@sdu.edu.cn

This file includes:

S1. Materials

S2. Experimental Section

S3. Material Characterizations

S4. Electrochemical Measurements

S5. DFT calculations

S6. Supplementary Figures S1-S20

S1. Materials

Zinc acetate dihydrate ($C_4H_6O_4Zn·2H_2O$), thioacetamide (C_2H_5NS, TAA), ethanediamine ($C_2H_8N_2$, EDA), and sodium sulfide ($Na_2S·9H_2O$) were purchased from Sinopharm Chemical Reagent Co., Ltd., China. Cadmium acetate dihydrate ($C_4H_6O_4Cd·2H_2O$) was purchased from Aladdin Reagent Co., Ltd. All the reagents were used as received.

S2. Experimental Section

Synthesis of twin $Cd_xZn_{1-x}S$-B: As a typical example, $Cd_{0.7}Zn_{0.3}S$-B was prepared by sequentially adding 7.0 mmol of $C_4H_6O_4Cd·2H_2O$, 3.0 mmol $C_4H_6O_4Zn·2H_2O$ and 12.5 mmol of TAA to a 30 ml aqueous solution containing 5 mL of EDA. After stirring for 30 min, the mixture was sealed in a 50 mL teflon-lined autoclave, and heated to 180 ^oC for 24 h. After cooling down, the product was separated by filtration, and dried at 80 ^oC for 12 h in a vacuum oven. Similarly, the other twin $Cd_xZn_{1-x}S$-B series samples could be obtained by adjusting the ratio of the precursors, specifically, $C_4H_6O_4Cd·2H_2O$ was adjusted to 1.0, 3.0, 5.0 and 9.0 mmol, respectively, and the corresponding $C_4H_6O_4Zn·2H_2O$ was adjusted to 9.0, 7.0, 5.0 and 1.0 mmol. The obtained samples were named $Cd_{0.1}Zn_{0.9}S$-B, $Cd_{0.3}Zn_{0.7}S$-B, $Cd_{0.5}Zn_{0.5}S$-B, and $Cd_{0.9}Zn_{0.1}S$-B, respectively.

As a comparison, $Cd_{0.7}Zn_{0.3}S$ sample without twin boundary was prepared by changing the sulfur source to Na_2S and EDA was not added, and other conditions remained unchanged as the above preparation experiment. The preparation conditions of ZnS and CdS were the same as that of $Cd_{0.7}Zn_{0.3}S$-B, except that only Cd source and Zn source were added, respectively.

S3. Material Characterizations

X-ray diffraction (XRD) measurement was carried out on a Bruker D8-Advance X-ray powder diffractometer with a Cu-Kα radiation (λ=0.15418 nm). Scanning electron microscopy (SEM) images were collected using a Hitachi S-4800 microscope equipped with an energy dispersive X-ray analyzer (EDS, Horiba EMAX Energy EX-350). UV-vis diffuse reflectance spectroscopy (DRS) was conducted using a Shimadzu UV2550 recording spectrophotometer

equipped with an integrating sphere with wavelength of 200 nm to 900 nm. $BaSO_4$ was used as a reference. TEM and HRTEM images were obtained with a Philips Tecnai 20U-Twin microscope at an acceleration voltage of 200 kV. X-ray photoelectron spectroscopy (XPS, Thermo ESCALAB 250) was performed using monochromated Al-Kα radiation (1486.8 eV). High angle annular dark field images (HAADF AC-TEM) and EDX surface scans were taken by an FEI Titan with dual spherical aberration correctors and the microscope was operated at 300 kV.

S4. Electrochemical Measurements

The electrodes were fabricated by mixing 80% the active materials, 10% acetylene black, and 10% polyvinylidene difluoride (PVDF) dissolved in N-methyl-2-pyrrolidine (NMP). The mixed slurry uniformly pasted on copper foil and dried at 110 °C under vacuum for 10 h. The accurate mass loadings of the active materials were controlled in the range of 0.8-1.2 mg cm^{-2}.

For LIBs, 1 M $LiPF_6$ in EC: DMC: EMC (1:1:1, wt%) with 2.0% FEC was utilized as electrolyte. 2032-type coin cells were then assembled in a glove box filled with Ar (oxygen and moisture less than 1 ppm) using polypropylene film (Celgard 2320) as the separator. For the half-cell, pure Li metal was used as the counter electrode. The coin-type full battery was assembled using commercial $LiFePO_4$ as the cathode, and 1 M $LiPF_6$ in EC: DMC: EMC (1:1:1, wt%) with 2.0% FEC used as the electrolyte. The cathode electrode was prepared by mixing $LiFePO_4$, acetylene black, and polyvinylidene fluoride (PVDF) in a weight ratio of 8:1:1, followed by coating on aluminum foil. Prior to full-cell fabrication, the $Cd_{0.7}Zn_{0.3}S$-B anode was electrochemically activated by prelithiation, which was implemented by cycling it against a Li foil to eliminate the initial irreversible capacity. We take the reversible capacity of $Cd_{0.7}Zn_{0.3}S$-B in the first cycle (594.7 mA h g^{-1}) and the capacity of $LiFePO_4$ after stable cycle (84.0 mA h g^{-1}) as reference, the value for N/P=1.15, which described as equation of (S-1). The mass loading for the cathode was determined to about 2.58 mg cm^{-2} and the anode was about

0.42 mg cm^{-2}. The full-cells of $Cd_{0.7}Zn_{0.3}S$-B||$LiFePO_4$ were tested between 2.5 and 4.0 V (vs Li^+/Li) at room temperature. The capacity is calculated based on the mass of the $Cd_{0.7}Zn_{0.3}S$-B.

$$\frac{N}{P} = \frac{capacity\ contributed\ by\ anode}{capacity\ contributed\ by\ cathode} = \frac{reversible\ specific\ capacity\ of\ anode}{reversible\ specific\ capacity\ of\ cathode}$$
$$= \frac{594.7\ mA\ h\ g^{-1} * 0.42\ mg\ cm^{-2}}{84.0\ mA\ h\ g^{-1} * 2.58\ mg\ cm^{-2}}$$
$$= 1.15 \qquad (S-1)$$

For the SIBs, Na metal is the counter and reference electrode in the half cells. The glass microfibers of Whatman GF/D acted as the separator and $NaClO_4$ (1.0 M) in ethylene carbonate (EC) and diethyl carbonate (DEC) (volume ratio of 1:1) with 5.0 wt % Fluoroethylene Carbonate (FEC) adding acted as electrolyte. The coin-type full battery was assembled using the as-obtained $NaNi_{0.45}Cu_{0.05}Mn_{0.4}Ti_{0.1}$ (NaNCMT) as the cathode, and the $Cd_{0.7}Zn_{0.3}S$-B anode was electrochemically activated by presodiation. The full-cells of $Cd_{0.7}Zn_{0.3}S$-B||NaNCMT were tested between 2.0 and 4.0 V (vs Na^+/Na) at room temperature. The capacity is calculated based on the anode mass.

The charge-discharge tests were performed on a NEWARE battery measurement system between cut off voltages of 3 V and 0.01 V. The obtained specific capacities were calculated based on the total mass of the active materials. Cyclic voltammetry (CV) tests were carried out between 0.01 V and 3 V at different scan rates from 0.1 to 1.0 mV s^{-1} on a CHI760D electrochemical working station. Electrochemical impedance spectroscopy (EIS) patterns were recorded using a CHI760D electrochemical working station in the frequency range from 100 kHz to 0.01 Hz with amplitude of 5 mV.

S5. DFT calculations

All calculations were performed using the plane wave based periodic DFT method as implemented in the Vienna Ab Initio Simulation Package (VASP). The electron-ion interaction was described with the projector augmented wave (PAW) method. The electron exchange and correlation energies were treated within the generalized gradient approximation in the Perdew-Burke-Ernzerhof functional (GGA-PBE). The plane wave basis was set up to 500 eV. Computations were satisfied until the energy and force converged within 10^{-6} eV and 0.01 eV $Å^{-1}$, respectively.

The climb image nudged elastic band (CI-NEB) method with the limited-memory Broyden-Fletcher-Goldfarb-Shanno (LBFGS) optimizer was used to search the paths for the diffusion of Li^+ ions. The initial (reactant) and final (product) configurations were obtained from fully converged relaxation. Five of inserted images used in the CI-NEB calculations depended on the reaction coordinates between the reactant and product.

S6. Supplementary Figures S1-S20

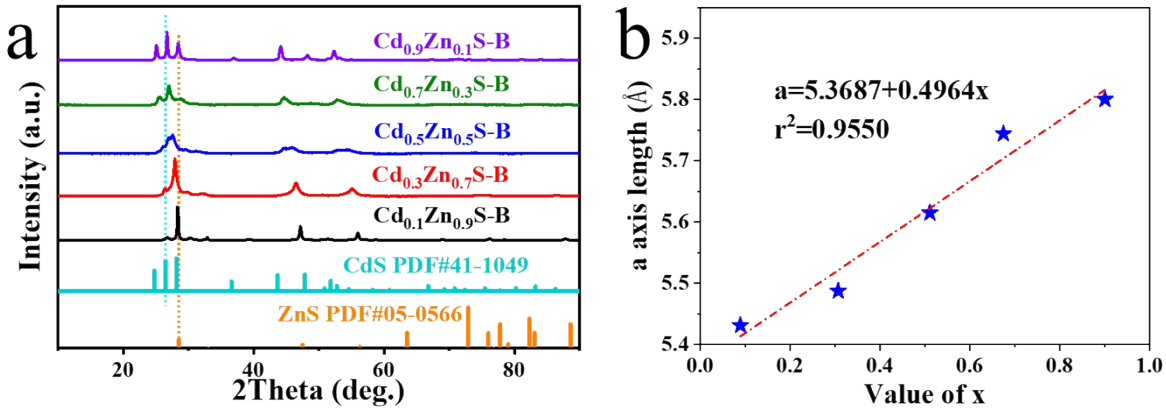

Fig. S1. (a) XRD patterns of $Cd_xZn_{1-x}S$-B series samples, CdS and ZnS. (b) The fitted line of lattice constants obtained from XRD patterns according to Vegard's law.

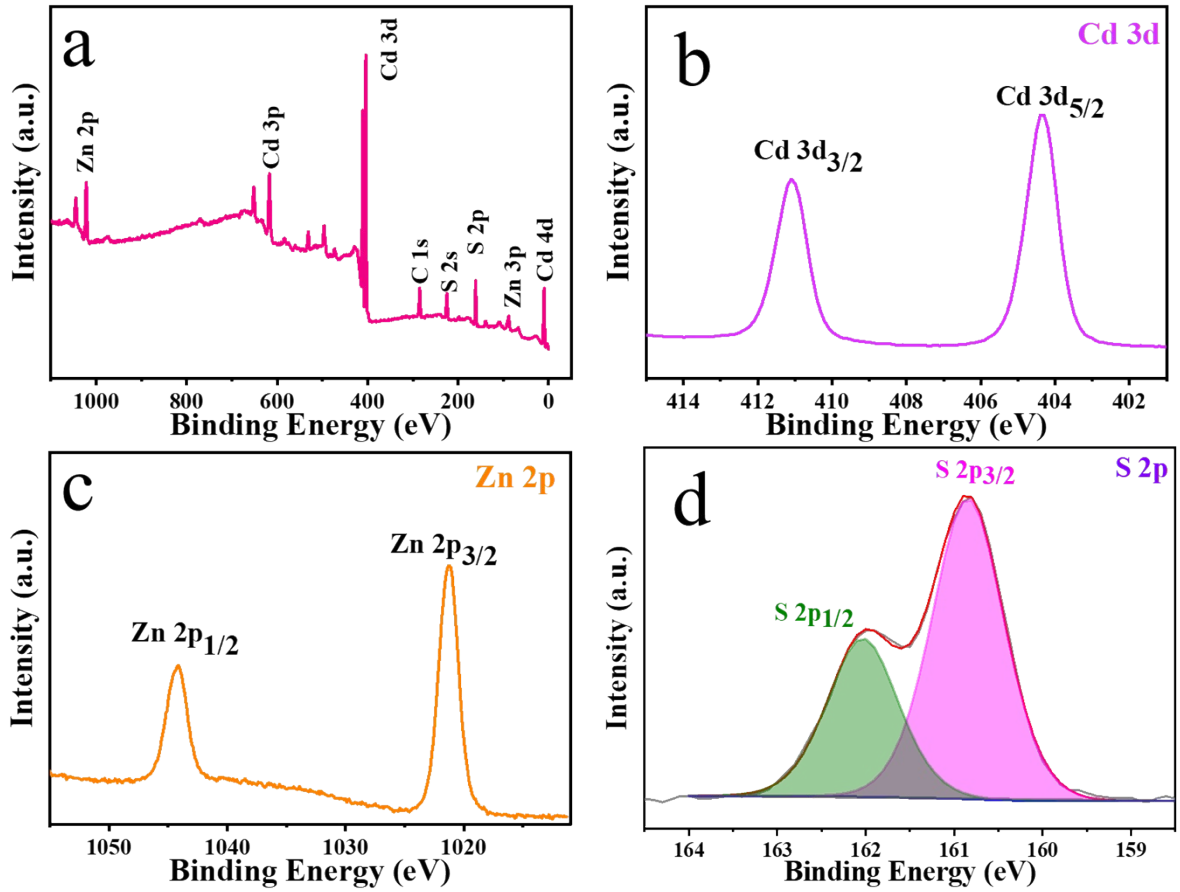

Fig. S2. (a) XPS survey of $Cd_{0.7}Zn_{0.3}S$-B. High-resolution XPS spectra of (b) Cd 3d, (c) Zn 2p and (d) S 2p for $Cd_{0.7}Zn_{0.3}S$-B.

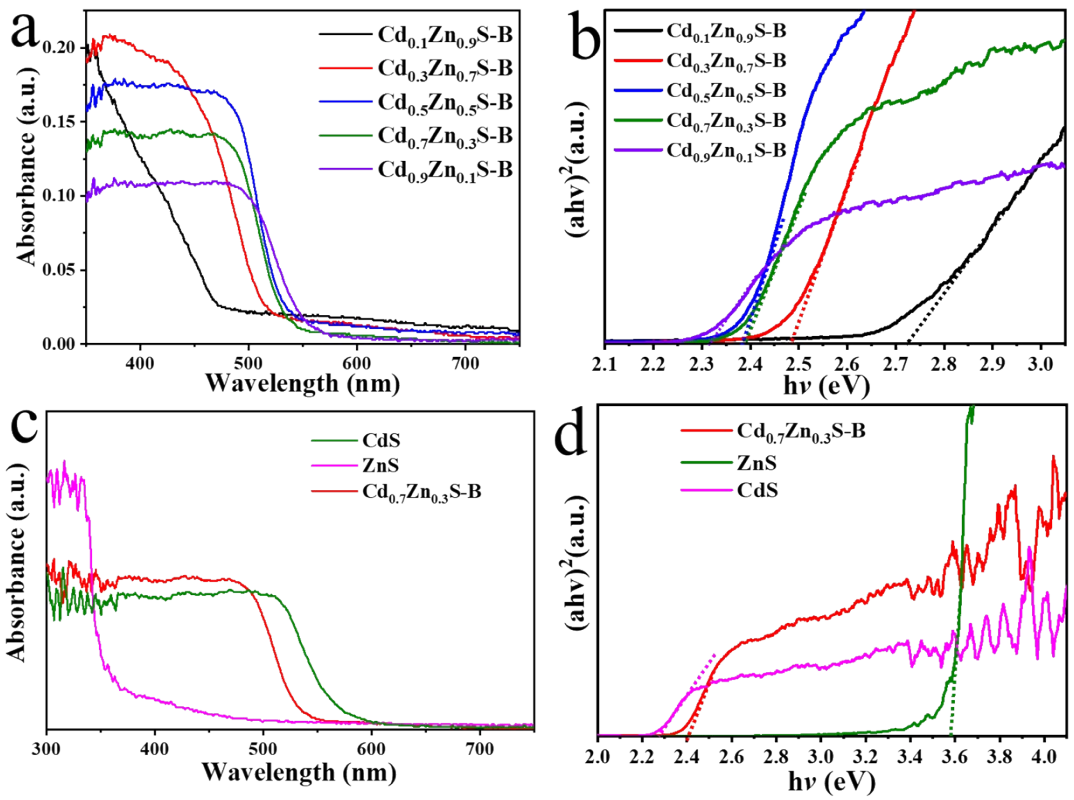

Fig. S3. UV-vis diffuse reflectance spectra and corresponding plots of transformed Kubelka-Munk function versus photon energy for (a, b) $Cd_xZn_{1-x}S$-B and (c, d) $Cd_{0.7}Zn_{0.3}S$-B, ZnS, and CdS.

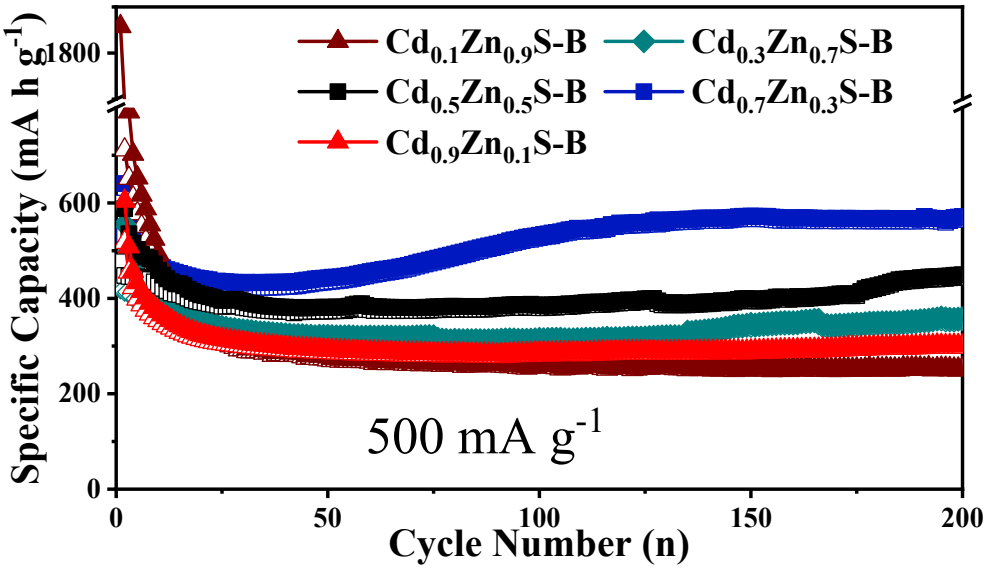

Fig. S4. Cycling performance at 500 mA g^{-1} for $Cd_xZn_{1-x}S$-B series samples.

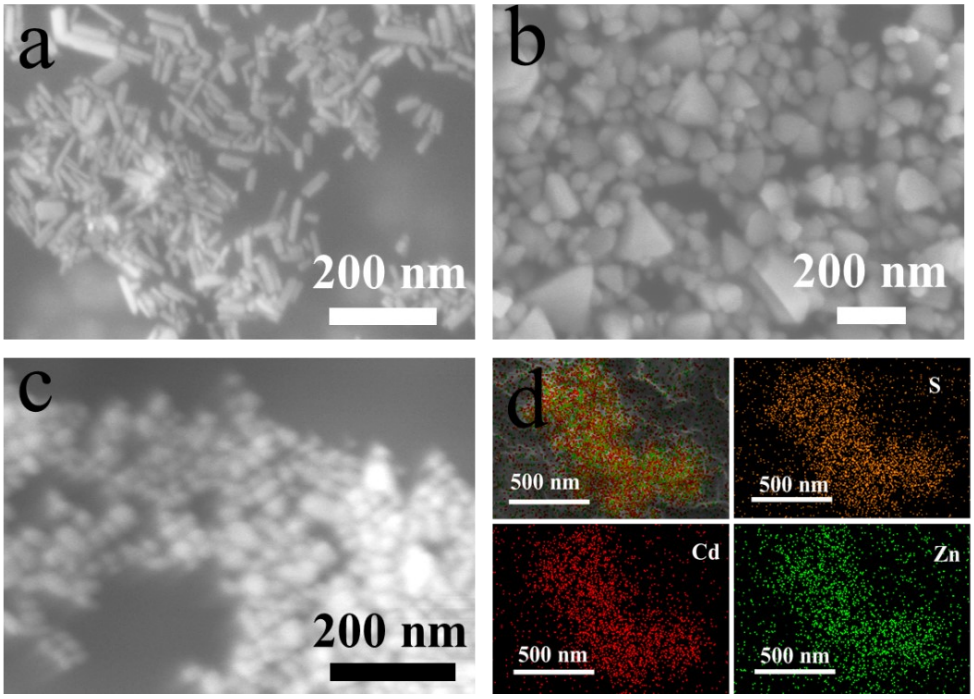

Fig. S5. SEM images of (a) ZnS, (b) CdS, and (c) $Cd_{0.7}Zn_{0.3}S$. (d) SEM image of $Cd_{0.7}Zn_{0.3}S$-B and corresponding EDS mapping.

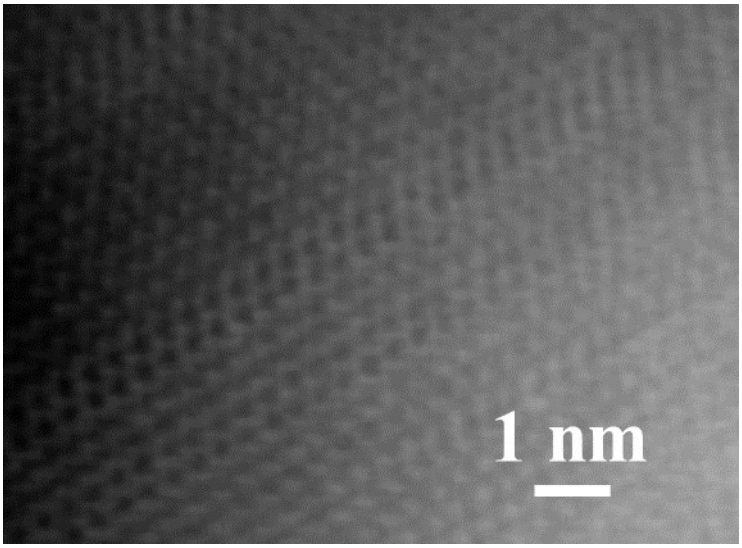

Fig. S6. The HAADF-STEM image of $Cd_{0.7}Zn_{0.3}S$-B.

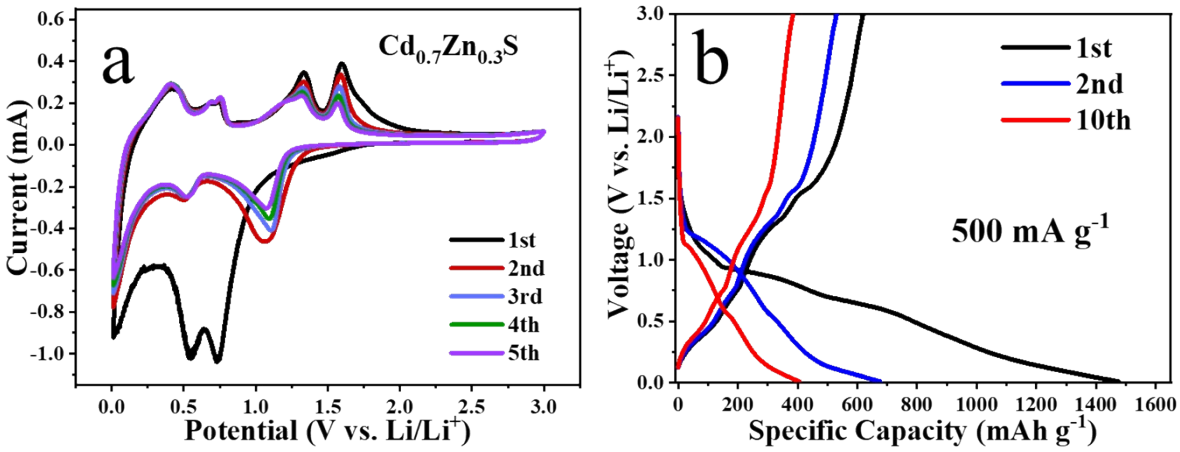

Fig. S7. (a) CV curves of the initial five cycles at 0.2 mV s^{-1} and (b) discharge-charge curves of different cycles at 200 mA g^{-1} for $Cd_{0.7}Zn_{0.3}S$.

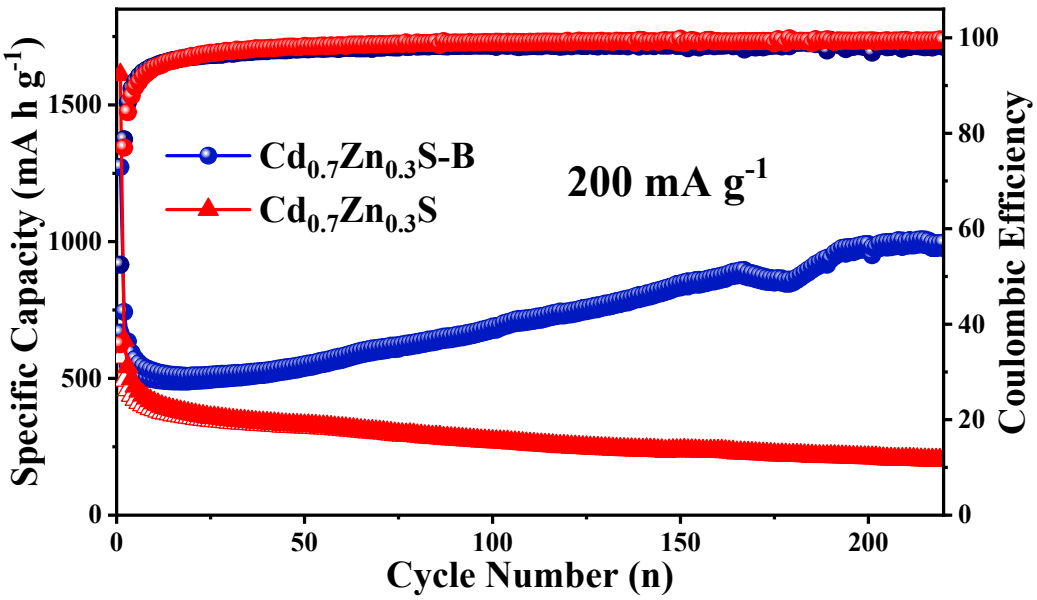

Fig. S8. Cycling performance at 200 mA g^{-1} for $Cd_{0.7}Zn_{0.3}S$ and $Cd_{0.7}Zn_{0.3}S$-B.

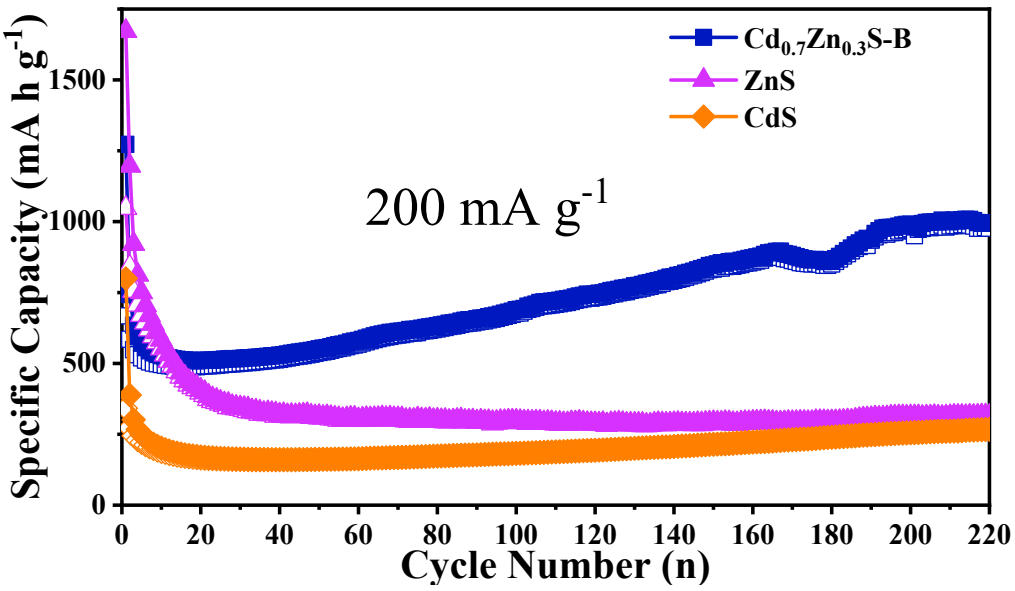

Fig. S9. Cycling performance at 200 mA g^{-1} for $Cd_{0.7}Zn_{0.3}S$-B, ZnS and CdS.

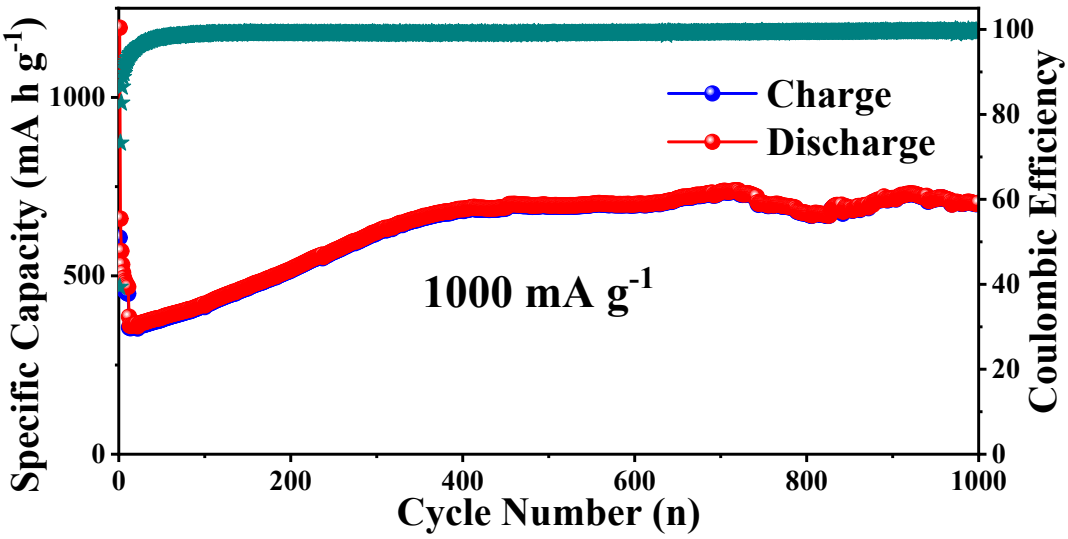

Fig. S10. Long-term cycling performance of $Cd_{0.7}Zn_{0.3}S$-B at a current rate of 1.0 A g^{-1}.

The reasons for the specific capacity of $Cd_{0.7}Zn_{0.3}S$-B continue to ascend with the increase of cycle number as follows. In the initial activation process, the gradual penetration of electrolyte increases the contact with active materials. In addition, the structure of the electrode material will change during the activation cycling process, exposing more active sites for further lithium storage, resulting in an increase in capacity. This phenomenon has been reported in the published literatures[1-3].

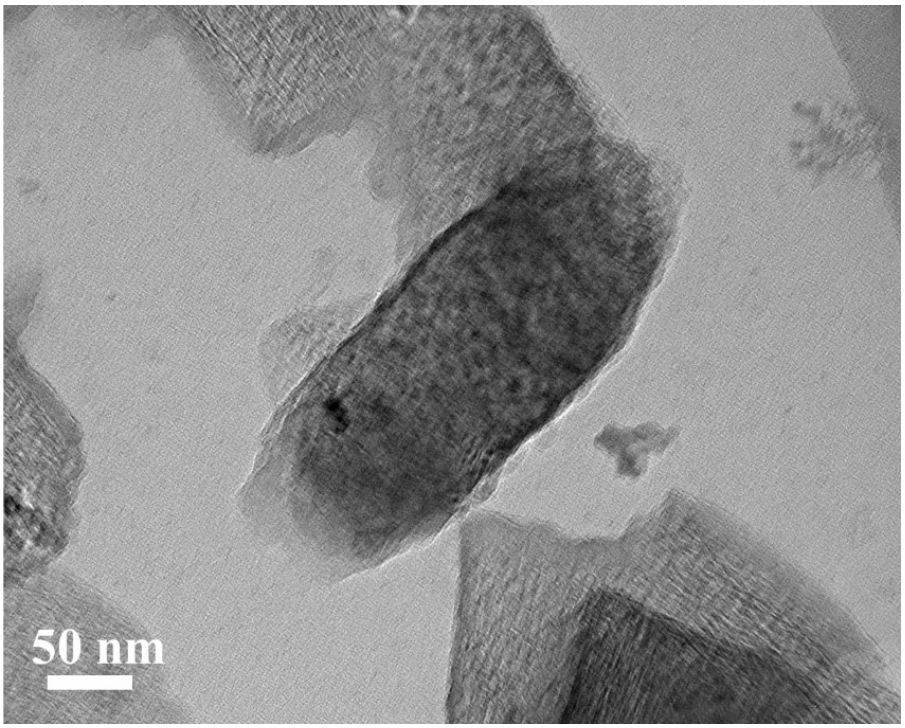

Fig. S11. TEM image of the $Cd_{0.7}Zn_{0.3}S$-B after 150 cycles.

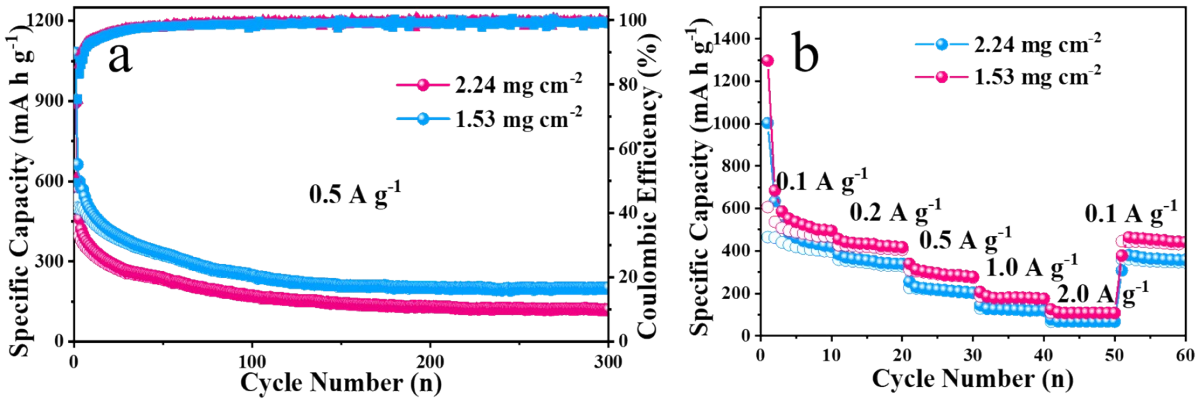

Fig. S12. (a) Cycling performance at 0.5 A g^{-1} and (b) rate capabilities for $Cd_{0.7}Zn_{0.3}S$-B with high areal mass loading of 1.53 and 2.24 mg cm^{-2}.

In order to test the practical application potential for $Cd_{0.7}Zn_{0.3}S$-B, electrodes with high mass loadings were fabricated. **Fig. S12** shows the electrochemical performance of $Cd_{0.7}Zn_{0.3}S$-B with a mass loading of 1.53 and 2.24 mg cm^{-2}, respectively. **Fig. S12**a presents that $Cd_{0.7}Zn_{0.3}S$-B can charge-discharge 300 cycles stablely at 0.5 A g^{-1} and maintain a high capacity of 120.7 mA h g^{-1} with a mass loading of 1.53 mg cm^{-2}. When the mass loading increased to 2.24 mg cm^{-2}, its capacity can be kept at 120.7 mA h g^{-1}. The rate capabilities of $Cd_{0.7}Zn_{0.3}S$-B with different mass loads are shown in **Fig. S12**b, and $Cd_{0.7}Zn_{0.3}S$-B with a mass loading of 1.53 mg cm^{-2} can deliver an average discharge capacity of 619.0, 432.1, 297.3, 182.2 and 110.5 mA h g^{-1} at a current density of 0.1, 0.2, 0.5, 1.0 and 2.0 A g^{-1}, respectively. A reversible capacity of 445.0 mA h g^{-1} can be maintained when the current density returned to 0.1 A g^{-1}. Even with a mass loading of 2.24 mg cm^{-2}, an average discharge capacity of 526.9, 355.2, 219.7, 125.2 and 68.4 mA h g^{-1} at a current density of 0.1, 0.2, 0.5, 1.0 and 2.0 A g^{-1}, respectively. The above data show that $Cd_{0.7}Zn_{0.3}S$-B possesses high practical application potential.

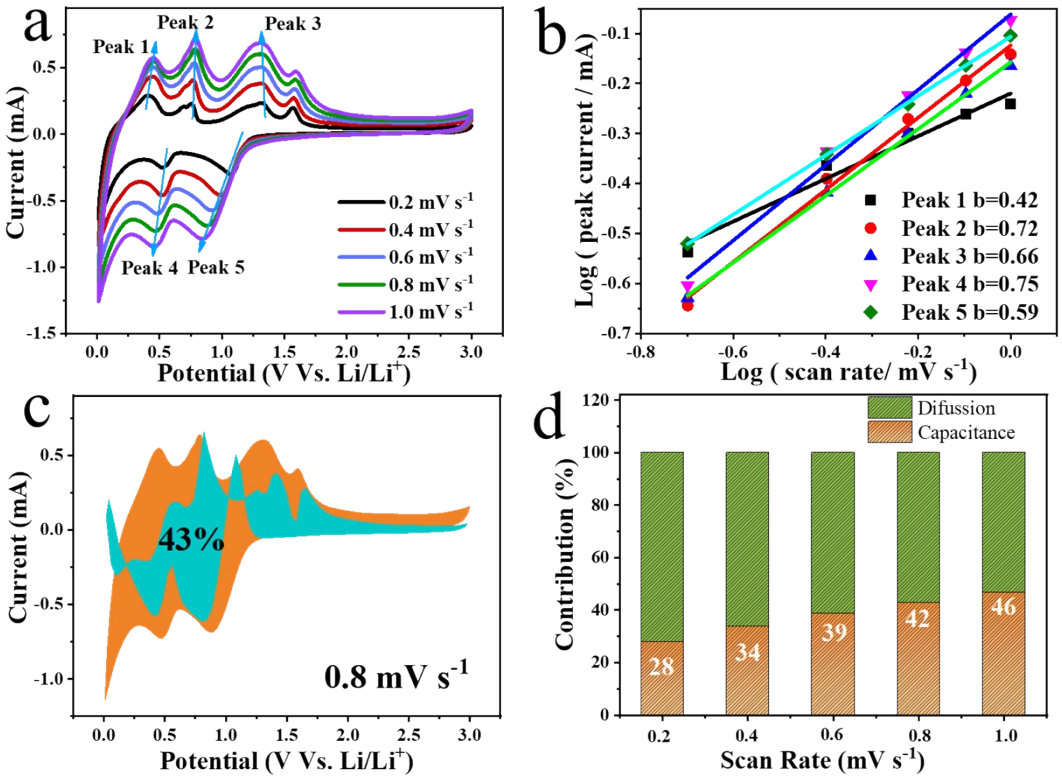

Fig. S13. (a) CV curves of $Cd_{0.7}Zn_{0.3}S$ measured at 0.2-1.0 mV s^{-1} and (b) the corresponding linear relationship of log(*v*)-log(*i*) for lithiation/delithiation peaks. (c) CV profiles of the capacitance contribution ratio at 0.8 mV s^{-1} for $Cd_{0.7}Zn_{0.3}S$ and (d) the capacitive contribution at different scan rates for $Cd_{0.7}Zn_{0.3}S$.

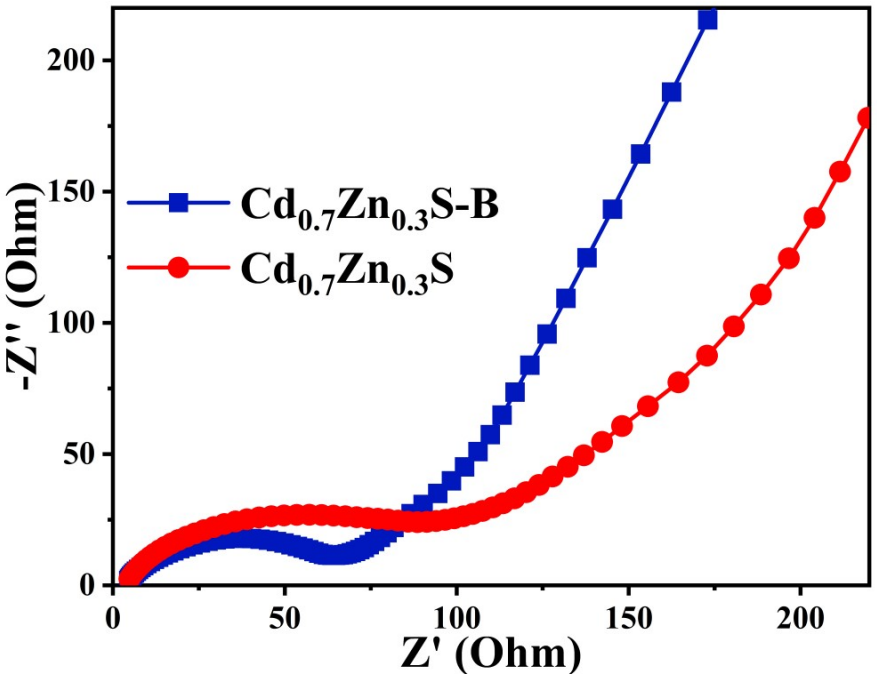

Fig. S14. EIS curves for $Cd_{0.7}Zn_{0.3}S$ and $Cd_{0.7}Zn_{0.3}S$-B after 200 cycles.

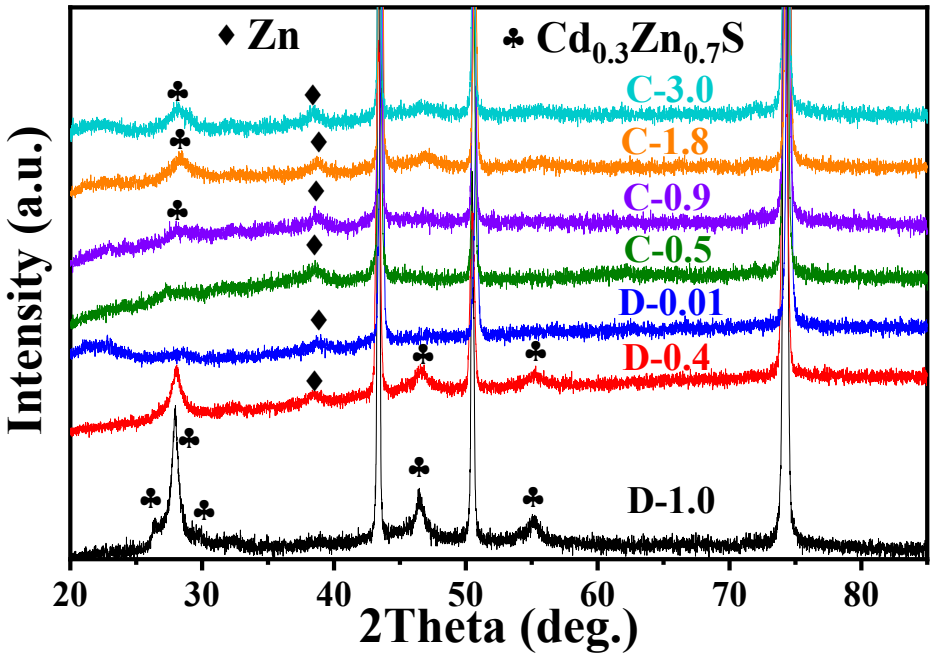

Fig. S15. *Ex*-situ XRD patterns of $Cd_{0.3}Zn_{0.7}S$-B electrode under different discharge/charge states.

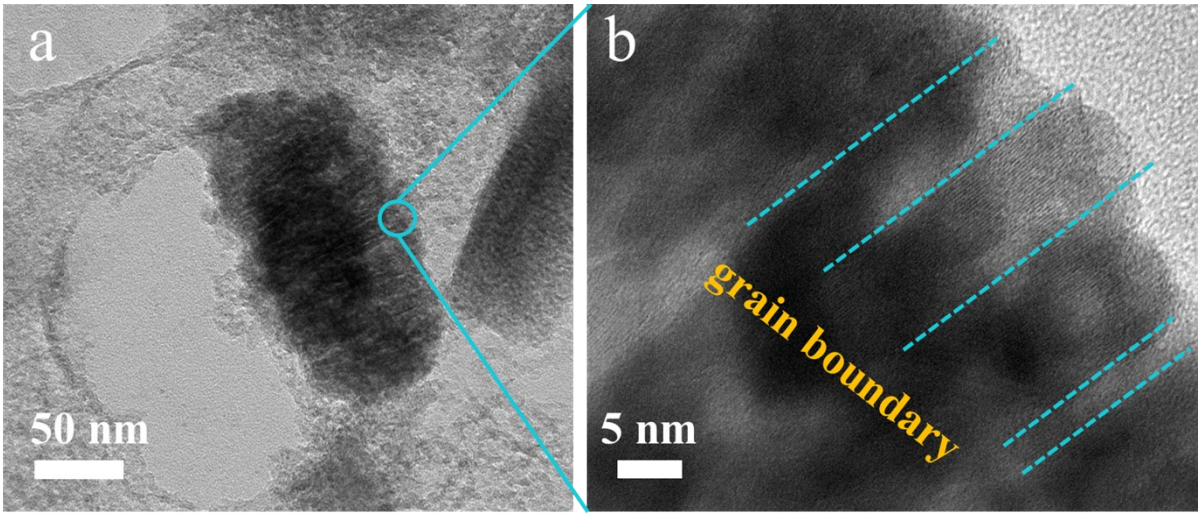

Fig. S16. (a) TEM and (b) HRTEM image of the $Cd_{0.7}Zn_{0.3}S$-B after charging to 3 V in the first discharging process.

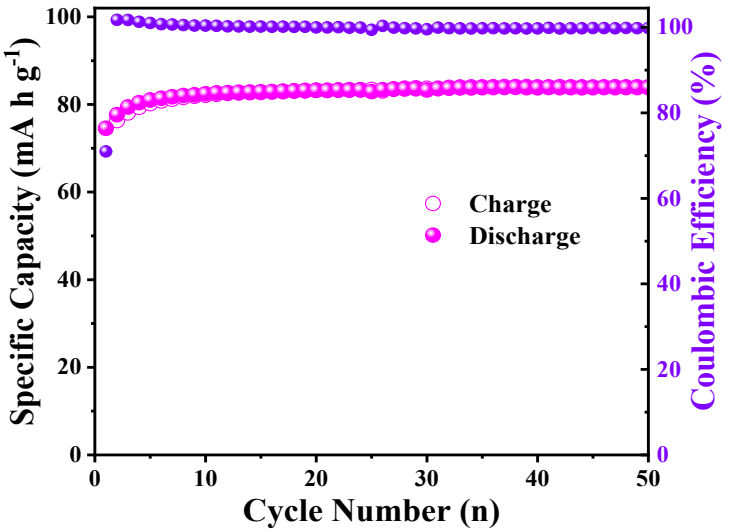

Fig. S17. Cycling performance of $LiFePO_4$ electrode with a mass loading of 2.58 mg cm^{-2} at 0.5 A g^{-1}.

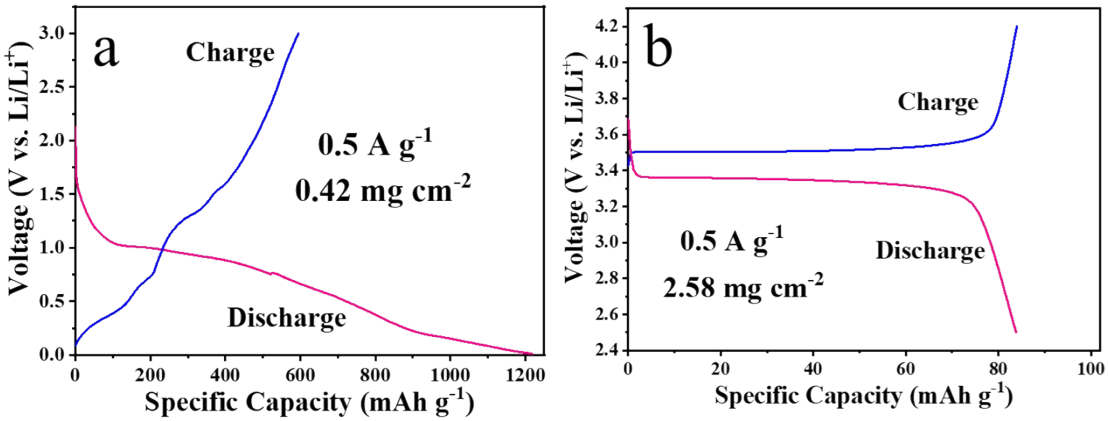

Fig. S18. Charge-discharge curves of (a) $Cd_{0.7}Zn_{0.3}S$-B anode and (b) $LiFePO_4$ cathode electrode material at 0.5 Ag^{-1}.

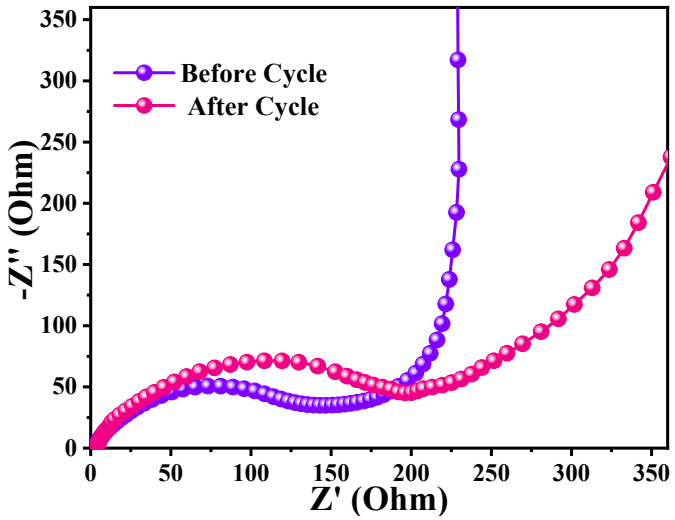

Fig. S19. EIS curves for $Cd_{0.7}Zn_{0.3}S$-B before and after cycle.

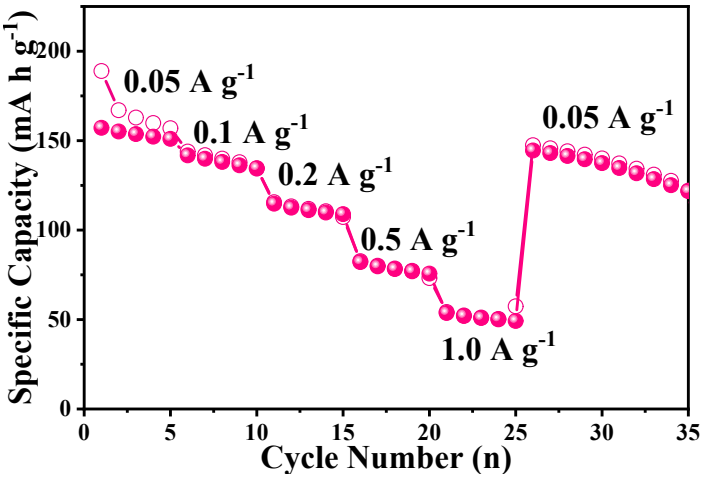

Fig. S20. Rate capabilities of $Cd_{0.7}Zn_{0.3}S$-B||NaNCMT full cell.

References

[1] H. Jiang, Y. Gan, J. Liu, X. Wang, R. Ma, J. Liu, and J. Wang, *J. Mater. Chem. A*, 2022, **10,** 9468-9481.

[2] X. Jin, H. Huang, A. Wu, S. Gao, M. Lei, J. Zhao, X. Gao, and G. Cao, *ACS Nano* 2018, **12**, 8037-8047.

[3] R. Hu, Y. Ouyang, T. Liang, H. Wang, J. Liu, J. Chen, C. Yang, L. Yang, and M. Zhu, *Adv. Mater.* 2017, **29**, 1605006.